Journal of Rock Mechanics and Geotechnical Engineering 8 (2016) 499–512

Contents lists available at ScienceDirect

Journal of Rock Mechanics and Geotechnical Engineering

journal homepage: www.rockgeotech.org

Full length article

Key technologies and risk management of deep tunnel construction at Jinping II hydropower station

Chunsheng Zhang*, Ning Liu, Weijiang Chu

HydroChina Huadong Engineering Corporation, Hangzhou, 310014, China

ARTICLE INFO

Article history:
Received 16 June 2015
Received in revised form
8 September 2015
Accepted 8 October 2015
Available online 1 May 2016

Keywords:
Jinping II hydropower station
Deep tunnels
High geostress
High external water pressure
Rockburst
Groundwater

ABSTRACT

The four diversion tunnels at Jinping II hydropower station represent the deepest underground project yet conducted in China, with an overburden depth of 1500–2000 m and a maximum depth of 2525 m. The tunnel structure was subjected to a maximum external water pressure of 10.22 MPa and the maximum single-point groundwater inflow of 7.3 m^3/s. The success of the project construction was related to numerous challenging issues such as the stability of the rock mass surrounding the deep tunnels, strong rockburst prevention and control, and the treatment of high-pressure, large-volume groundwater infiltration. During the construction period, a series of new technologies was developed for the purpose of risk control in the deep tunnel project. Nondestructive sampling and in-situ measurement technologies were employed to fully characterize the formation and development of excavation damaged zones (EDZs), and to evaluate the mechanical behaviors of deep rocks. The time effect of marble fracture propagation, the brittle–ductile–plastic transition of marble, and the temporal development of rock mass fracture and damage induced by high geostress were characterized. The safe construction of deep tunnels was achieved under a high risk of strong rockburst using active measures, a support system comprised of lining, grouting, and external water pressure reduction techniques that addressed the coupled effect of high geostress, high external water pressure, and a comprehensive early-warning system. A complete set of technologies for the treatment of high-pressure and large-volume groundwater infiltration was developed. Monitoring results indicated that the Jinping II hydropower station has been generally stable since it was put into operation in 2014.

1. Introduction

The Jinping II hydropower station is located at the Jinping bend on the Yalong River, which is at the junction of three counties (Muli, Yanyuan, and Mianning) in the Liangshan Yi Autonomous Prefecture of Sichuan Province, China. The course of the river bend itself is about 150 km in length as it winds around Jinping Mountain, over which the elevation drops 310 m. However, if passing directly through the mountain, the distance between the two sides of the bend is only about 16 km. To take advantage of this beneficial condition for hydroelectric production, the Yalong River is diverted through four diversion tunnels passing through the mountain. The Jinping II hydropower station consists of three major parts: the sluice, the diversion system, and the underground powerhouse, as illustrated in Fig. 1. This hydropower station is a low-gate, long-tunnel, and large-capacity diversion-type power station with a total installed capacity of 4800 MW. The total excavation volume of the underground construction in this project is approximately 13.2×10^6 m^3. The diversion tunnels, powerhouse chambers, transportation tunnels, adits, drainage tunnels, and other tunnels cross each other and form an enormously complex large-scale group of tunnels.

The Jinping II hydropower station is composed of seven parallel tunnels, including the four diversion tunnels, two auxiliary tunnels, and one drainage tunnel. Each of the tunnels is approximately 16.67 km in length, and the total length of the tunnels is approximately 118 km. The tunnel boring machine (TBM) was employed in the excavation of diversion tunnels #1 and #3 and the drainage tunnel, while drilling-and-blasting (DB) method was applied to the excavation of diversion tunnels #2 and #4 and the two auxiliary tunnels. The axes of the four diversion tunnels are nearly orthogonal to the ridge axis of Jinping Mountain, as illustrated in Fig. 2. The mountain drops steeply from its ridge axis with a large overburden, where 76.7% of the overburden has a depth greater than 1500 m

* Corresponding author. Tel.: +86 571 56738306.
E-mail address: zhang_cs@ecidi.com (C. Zhang).

Peer review under responsibility of Institute of Rock and Soil Mechanics, Chinese Academy of Sciences.

http://dx.doi.org/10.1016/j.jrmge.2015.10.010

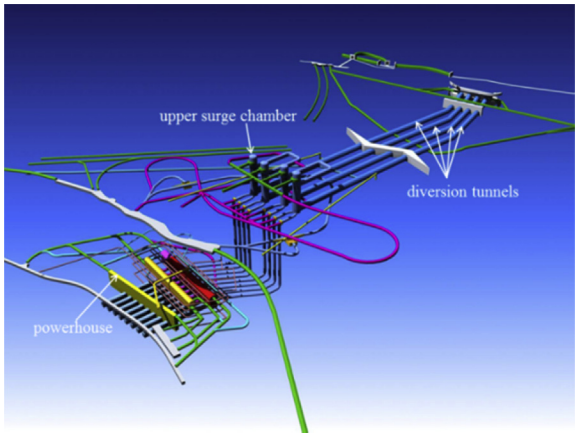

Fig. 1. Three-dimensional (3D) schematic diagram of the overall Jinping II project.

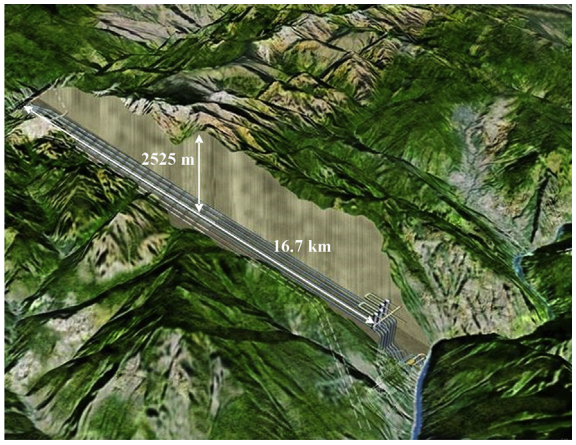

Fig. 2. The profile of the Jinping II deep tunnel group.

with a maximum depth of 2525 m, which is greater than the maximum depth of the Simplon Tunnel (2135 m), but slightly smaller than that of the Sarrans hydroelectric power station in France (2619 m). The excavation diameters of the tunnels of the Jinping II hydropower station are 12.4–14.6 m, which are considerably greater than that of the Sarrans project (5.8 m) (Zhang, 2007).

The hydrogeological conditions along the deep tunnel group axis of the Jinping II hydropower station are quite complex. As illustrated in Fig. 3, the primary rock material found along the tunnel group is Triassic marble, followed by sandstone, and a segment of green schist hundreds of meters in length. According to an investigation conducted in the auxiliary tunnel, the marble of different ages has varying characteristics, and the marble of the Baishan group has better integrity and stronger brittle characteristics. The maximum geostress measured in the field was 113.87 MPa, and the ratio of the minimum strength of the surrounding rocks to the geostress was 0.8. A large volume of karst groundwater with ultra-high pressure was found in the alpine-gorge region, where the maximum external water pressure was 10.22 MPa, with a maximum single-point groundwater inflow rate of 7.3 m^3/s.

The major technical difficulties involved the stability of the tunnels and the permeability controlling of the surrounding rocks under high geostress and high external water pressure conditions. The challenges such as the prevention and control of strong rockburst, and the specialized treatments required for high external water pressure and large-volume groundwater infiltration are rarely reported. Therefore, the possibility for a successful completion of this project was considered questionable by many at the beginning. In this circumstance, the HydroChina Huadong Engineering Corporation began to excavate a 5 km-long test tunnel in 1991 in order to provide technical support for the safe construction and operation of this project. By the end of 1995, the length of this test tunnel was 4.168 km. In addition, two parallel auxiliary tunnels were excavated at the elevation of the diversion tunnels for the purposes of transportation, prospecting, and testing. The present paper focuses on the prevention and control of strong rockburst and groundwater treatments.

2. Mechanical behaviors of deep marble

Due to the unfavorable geological structures, the high geostress has a considerable effect on the structural stability of the surrounding rocks. Moreover, the secondary stress concentration of rocks in the high-geostress field after excavation further contributes to the complexity of the stress environment. Finally, the high external water pressure poses a substantial challenge to the safe and stable operation of the deep tunnel group. To understand the mechanical behaviors of deep marble, various mechanical tests and numerical simulations during excavation in response to the site-specific geological conditions were conducted. Based on the data acquired during excavation, the models and methods were improved to ensure the safety of the tunnels during operation.

2.1. Testing technologies for determination of the characteristics of deep rocks

For stress relief of rocks during excavation in high geostress condition, rocks exhibit complex mechanical responses. Understanding the mechanical behaviors of deep rocks is the fundamental issue in deep rock engineering. For this, a number of tests on deep rocks of Jinping II project were conducted.

2.1.1. Nondestructive sampling technique

Because the strength of the on-site marble is relatively low and the initial geostress is relatively high, the rock is prone to damage in the sampling process. Fig. 4 shows the recorded acoustic emission (AE) events with respect to axial compressive stress for an on-site

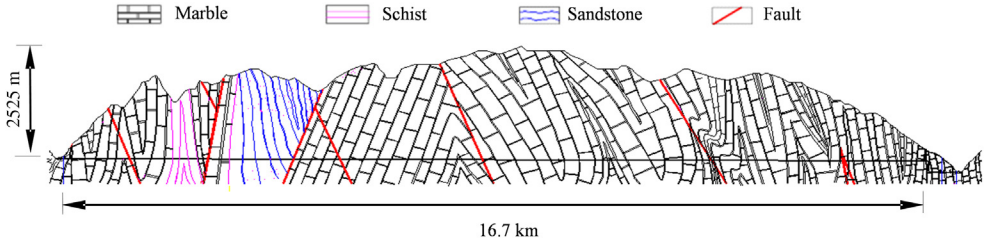

Fig. 3. Simplified geological profile along the tunnel axis.

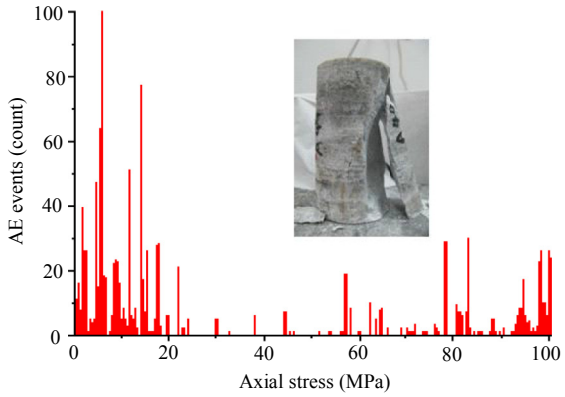

Fig. 4. AE events recorded in the compression process of marble sample.

marble sample obtained at a depth of approximately 2000 m using the conventional drilling method. When the axial compressive stress is less than 20 MPa, the rock sample exhibits a clear compression phenomenon, and notable AE events appear at the early stage of testing. Obviously, in addition to the initial transverse damage existing in the sample, some cracks nearly parallel to the direction of applied compressive stress also exist, which lead to a rapid increase in AE events. This indicates that rock samples obtained at that depth using the conventional method generally have initial damage. The distribution of the initial damage can affect the mechanical behaviors and failure modes of the rock samples (Liu et al., 2012a).

Fig. 5 shows a schematic diagram of the developed nondestructive sampling technique (Liu et al., 2012b). With this technique, the stress distributions in the rock mass of the sampling area are adequately adjusted by drilling several holes one by one in order to avoid damage to the rock sample. Figs. 6 and 7 respectively show the recorded AE events with respect to the axial compressive stress for on-site marble samples obtained at a depth of approximately 2000 m using the developed nondestructive sampling technique. The former rock sample was obtained from a stress-relief hole and the latter was obtained from a sampling hole (Liu et al., 2012b). In Fig. 6, at the early stage of the test, AE events are evidently concentrated, demonstrating the existence of initial

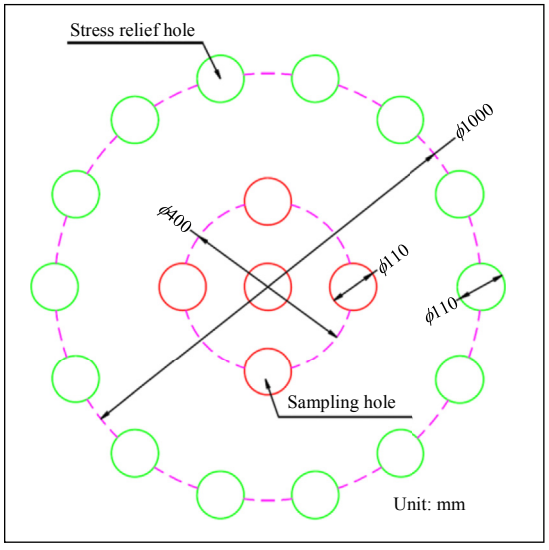

Fig. 5. The improved nondestructive sampling method.

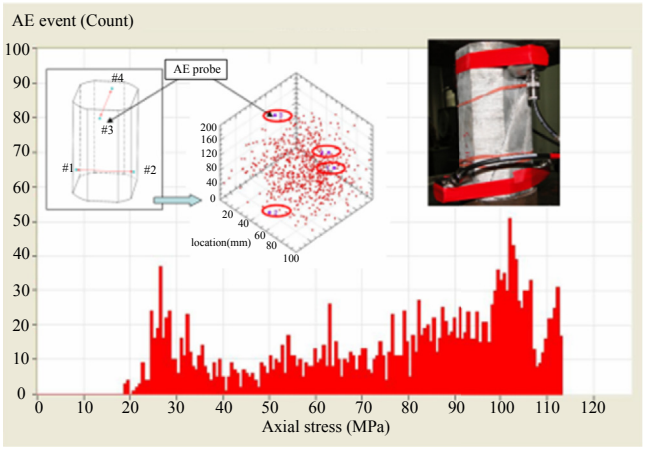

Fig. 6. AE events versus axial stress of a rock core obtained from a stress-relief hole.

damage. This is similar to the test result given in Fig. 4. The peak strength is 103 MPa. However, relatively few initial AE events are observed in Fig. 7, and the first AE event peak appears at a stress of 90 MPa, approximately 70%–80% of the peak strength of the rock. The rock failure occurs at a stress of 118 MPa, which is greater than the strength of the rock core obtained from the stress-relief hole.

2.1.2. *In-situ testing techniques*

The laboratory test can provide the mechanical behaviors of small-scale rock samples. However, because the rocks have notable differences at different scales, large-scale in-situ tests are required to properly evaluate the mechanical behaviors of rock masses on large scale (Zhang et al., 2014).

Due to the specific stress environments and mechanical behaviors of deep marble at the Jinping II project site, the mechanical responses of rocks after tunnel excavation are substantially different from those under the original conditions. The types of damages to the deep brittle marble include rockburst, spalling, and fracture-induced damage, which occur under the conditions of very small deformation, making deformation-based methods inapplicable for evaluating and predicting the stability and safety of the surrounding rocks. By comparison, the direct monitoring of surrounding rock stress and fracture (AE or microseismic events) is of practical significance. Data obtained by these methods provide key information for determining the mechanical characteristics of rock mass.

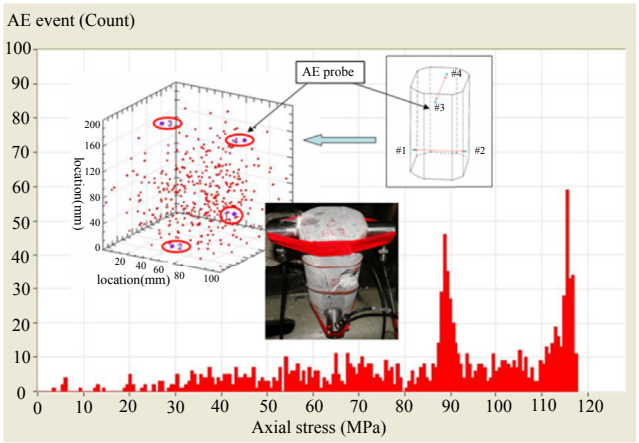

Fig. 7. AE events versus axial stress of a rock core obtained from a sampling hole.

The in-situ pilot tests were conducted with a focus on two aspects. The first one is the stress change and the final state of the surrounding rock stress in the stress concentration area, and the second is the fracture development and the final state of the rock mass that occurs in conjunction with the changes in the surrounding rock stress. These two aspects are the main contents of monitoring optimization. The in-situ test area is arranged near transverse tunnel #2 at a depth of approximately 1850 m, as shown in Fig. 8. A testing adit approximately 50 m in length (denoted as the monitoring tunnel in Fig. 8) was bored perpendicular to the transverse tunnel, and therefore, parallel with the diversion tunnels, wherein the monitoring instruments were installed for recording the responses of the surrounding rocks during excavation of diversion tunnel #3 as the TBM approached, passed through, and moved away from the test area (Chu et al., 2014). The specific monitoring techniques employed are described as follows:

(1) Stress monitoring: The stress state of the surrounding rocks during the tunnel excavation process was monitored to provide basic data for studying the rock strength.
(2) AE monitoring: The positions and scope of micro-fractures occurring during the stress adjustment of the rocks surrounding the diversion tunnel were investigated to study the rock damage (Chen et al., 2010).
(3) Wave velocity testing: Testing was conducted to determine the excavation damaged zone (EDZ) and the position and scope of the high stress area.
(4) Monitoring of rock deformation: The surrounding rock deformation was evaluated by multipoint displacement meter monitoring, and rock deformation was employed to determine the EDZ of the surrounding rocks in conjunction with the wave velocity test results.
(5) Digital borehole survey: Surveys were conducted to intuitively understand the macro-fracturing process in the surrounding rocks.

The in-situ tests showed that rock deformation, variations of the stress state, and microcrack initiation occur in the rock mass at a distance ahead of the excavation face, about 1.2 times the diameter of the diversion tunnel. The substantial changes in the stress state of the rock mass also occur 2–10 m behind the tunnel face. The AE data indicate that the greatest AE energy during tunneling is produced by the rock mass in a range from 5 m ahead of the tunnel face to 10 m behind the tunnel face, and the AE is basically stable when the tunnel face is 10 m ahead of the AE monitoring section. The results of optical fiber Bragg grating monitoring indicate that, in the zone close to the wall where the rock mass is seriously damaged, some superficial microcracks still generate after the impact of tunneling disappears. The most serious excavation-induced damage occurs on the right spandrel, and the EDZ has a depth of about 3 m. The results of the multipoint displacement meter monitoring show that the deformation of surrounding rocks during tunnel excavation is not significant.

Using in-situ pilot tests, we obtained an in-depth understanding regarding the process of change and the final state of the surrounding rock stresses, the spatial locations of fractures formed during adjustment of the surrounding rock stress, the displacements of the surrounding rocks, and the EDZ depths. The testing also provides first-hand data for assessing the stability of the surrounding rocks, and for optimizing the support design.

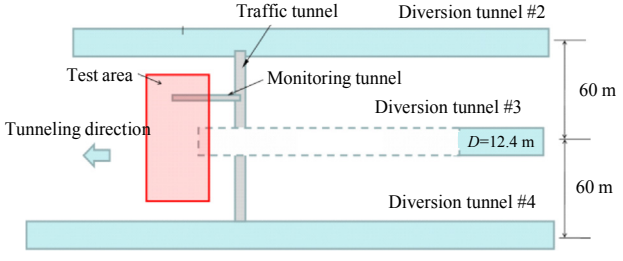

Fig. 8. Layout of the comprehensive in-situ testing conducted for large-scale rock masses.

2.2. Mechanical behaviors of deep marble

2.2.1. Brittle–ductile–plastic transition behaviors of deep marble

Under high geostress environments, the rock masses exhibit complex mechanical behaviors (Zhang et al., 2010a, b). Fig. 9 shows the triaxial stress-axial strain curves for marble samples with size of 100 mm × 50 mm of the Baishan group. It can be noted that the confining pressure has a significant e ffect on the post-peak mechanical behaviors of the marble samples, which can be characterized as follows (Zhang et al., 2011, 2014):

(1) As the confining pressure increases, the difference between the peak strength and residual strength decreases.
(2) When the confining pressure is larger than 10 MPa, the stress–strain curve does not drop rapidly after attaining the yield strength, but exhibits a notable feature of ductility.
(3) When the confining pressure is relatively high, the slope of the curve falling from the peak strength to the residual strength is substantially reduced.
(4) The brittle–ductile transition of the marble is highly sensitive to the level of the confining pressure. Generally, when the confining pressure is larger than 6 MPa, ductility features can be observed.
(5) At a relatively high confining pressure beyond the yield strength of the marble, the stress–strain curve is nearly representative of the mechanical behavior of a plastic-perfect material, and no notable stage of residual strength is observed.

A brittle–ductile–plastic model based on the Hoek–Brown failure criterion was developed to describe the brittle–ductile–plastic behaviors of deep marble, which are prominent with increasing confining pressure. The deformation and strength parameters employed to describe the brittle–ductile–plastic

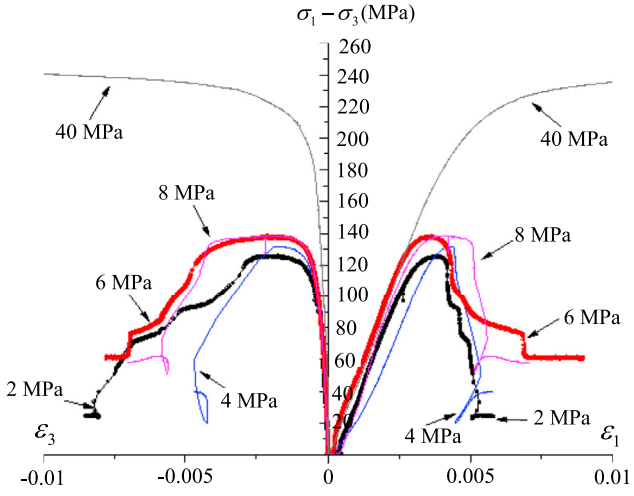

Fig. 9. Triaxial test results on marble of the Baishan group.

Table 1
The deformation and strength parameters used to describe the brittle–ductile–plastic behavior of deep marble.

Uniaxial compressive strength (MPa)	Young's modulus, E (GPa)	Poisson's ratio	m_b		s		a	
			Peak	Residual	Peak	Residual	Peak	Residual
140	60	0.27	9	10.5	1	0	0.5	0.65

Note: m_b, s and a are the material constants of the rock mass.

behaviors of deep marble are listed in Table 1. The FLAC^{3D} was employed to simulate the triaxial compression tests. The resulting axial stress-axial strain curves under different confining pressures are given in Fig. 10. As can be observed, when the confining pressure is 0, the stress–strain curve exhibits brittle behavior. When the confining pressure increases to 5 MPa, the model reflects the brittle–ductile behavior well. When the confining pressure increases to 30 MPa, the model can reflect the plastic behavior as expected.

2.2.2. Time effect of fracture propagation in deep marble

In hard rock tunnels under high geostress conditions, the scope of surrounding rock fracture and relaxation will continue to expand over a considerable period of time. This phenomenon is denoted as the time effect of fracture propagation, which is associated with the long-term strength of hard rock materials. Potyondy (2007) pointed out that the time effect of fracture propagation in the surrounding rocks is influenced by three factors, i.e. the nature of the rock, the level of stress applied, and the changes in environmental factors such as the humidity and the presence of water.

Static fatigue test was employed to evaluate the time effect of fracture propagation of deep marble samples. Static fatigue test consists of two operational stages, i.e. initial loading and constant loading. At the initial loading stage, the specimen is axially loaded to a constant stress value that is determined according to the laboratory test results of crack initiation. The axial load remains at this constant value during the constant loading stage until the specimen fails, and then the time to failure is recorded. Fig. 11 shows the results of fatigue failure testing on marble samples of the Yantang group. It can be observed that the time from initiation to failure varies according to the stresses applied, exhibiting the time effect of fracture propagation (Liu et al., 2012a).

According to the monitoring data obtained from the Jinping II project in association with corresponding numerical analyses and laboratory test results, the excavation of large cross-sectional hydraulic tunnels at great depth under high geostress conditions will result in fracture and damage to the surrounding rocks. In addition, the fracture propagation and strength of marble show significant time effects (Fairhurst, 2004; Liu et al., 2011a, b; 2013a, b; Zhang et al., 2013). Therefore, the use of reinforced concrete lining is required to improve the load bearing capacity of the surrounding rocks. However, a single reinforced concrete lining is insufficient to increase the bearing capacity of the surrounding rocks, thus grouting was employed in combination with the reinforced concrete lining in this project. This reinforcement method improves the anti-permeability of the surrounding rocks, allowing for the full utilization of the self-supporting capacity of the surrounding rocks. Optimizing the arrangement of pressure-relief holes on the outside of the lining allows the external water pressure and the force applied on the lining to be reduced, ensuring the long-term safety of the tunnel.

3. Combined load bearing system

The construction of the long, deep tunnels follows the principle that the stability of the surrounding rocks should primarily rely on their own self-supporting capacity. As such, the surrounding rocks serve as the main load bearing structure, and the measures

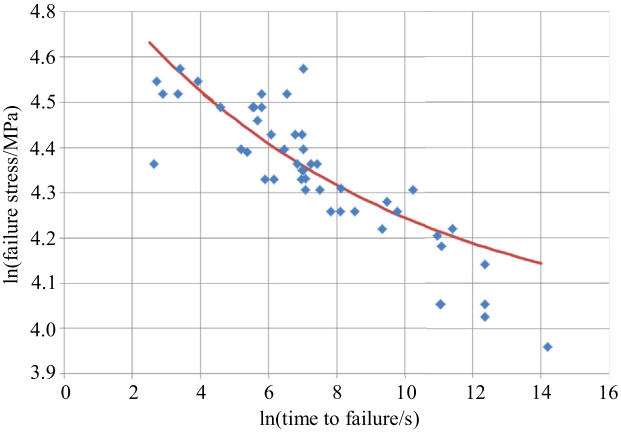

Fig. 11. Fatigue failure limit of marble of the Yantang group.

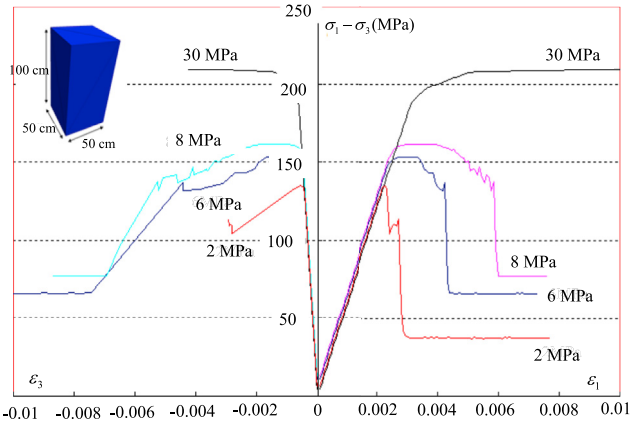

Fig. 10. Numerical results of the brittle–ductile–plastic transition.

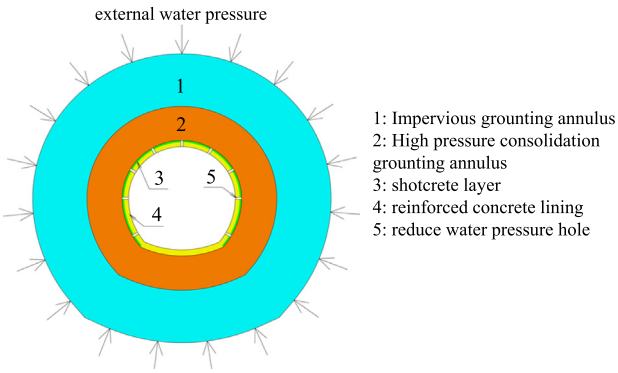

Fig. 12. The combined load bearing system.

Fig. 13. An example of fracture-induced damage to the surrounding rocks in a deep tunnel of the Jinping II project.

including anchor support and secondary high-pressure consolidation grouting are used to form the unified load bearing structure as illustrated in Fig. 12. This structure provides triaxial confining pressure on the surrounding rocks, and ensures their stability near the internal surface of the tunnel. In this circumstance, the surrounding rocks under the confining pressure are employed to bear the geostress caused by tunnel excavation, as well as ensure the safety and stability of the deep tunnels under high external water pressure.

A dynamic design method is followed in the practical design of the support structure. The pre-designed rock classification system and support parameters are used only as a reference in accordance with the geological and construction conditions revealed in the field. The support structure is actively optimized by combining data derived from on-site prototype monitoring and geophysical exploration, the results of field tests on new materials and new testing technologies, and analysis of surrounding rock fracture and damage.

3.1. The degree of surrounding rock damage and support depth

After deep tunnel excavation in the Jinping II project, the surrounding rocks exhibit deformation, fracture-induced damage, block failure, spalling, and rockburst. Among these responses, fracture-induced damage, as shown in Fig. 13, is the most common, and has the greatest impact on the support design.

The observed on-site failures of the surrounding rocks, including spalling, joints, and fractures, are all manifestations of the EDZ, and are also the primary basis for determining the fracture depth by visual inspection. The scale of cracks in the EDZ is much smaller than that in the fractured zone, and under normal circumstances, it is difficult to detect these types of cracks by visual

Table 2
Microscale properties of Jinping T_{2y}^5 marble.

Density (kg m^{-3})	Minimum diameter (mm)	Particle diameter ratio	Particle modulus (GPa)	Parallel bond strength (GPa)
2600	0.4	1.66	30	50
Stiffness ratio	Normal strength (MPa)	Tangential strength (MPa)		Initiation strength (MPa)
1.5	100 ± 20	80 ± 15		30

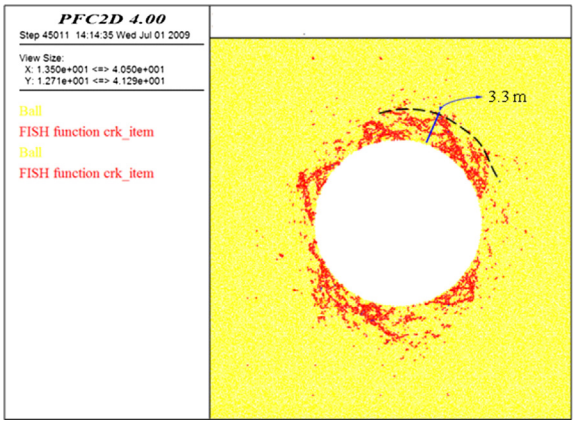

Fig. 14. Simulated damage distribution of surrounding rocks at a depth of 2000 m.

inspection. As such, special monitoring techniques such as acoustic testing must typically be adopted to determine the scope and depth of the damage (Read, 2004; Malmgren et al., 2007).

By comparing discontinuous and continuous discrete element methods for studying surrounding rock damage, we selected the discontinuous particle flow code (PFC) for analyzing the depth of fracture-induced damage in the surrounding rocks. The most prominent advantage of the PFC is that it can directly describe the evolution of internal rock damage. This is particularly important for the analysis of hard rock damage under high geostress conditions, facilitating the direct assessment and analysis of the EDZ, and the in-depth, systematic interpretation of the damage mechanism (Cai et al., 2001a; Martino and Chandler, 2004; Potyondy and Cundall, 2004; Liu et al., 2011a, b).

Table 2 lists the microscale properties of Jinping T_{2y}^5 marble employed in the simulations. Figs. 14 and 15 show the damage distributions of the surrounding rocks at depths of 2000 m and 2400 m, respectively. Table 3 summarizes the PFC calculation results of the EDZ depths for the surrounding marble at different excavation depths. It can be seen from Table 3 that the EDZ depth gradually increases with increasing excavation depth, but does not exceed 4.2 m at an excavation depth of 2500 m. The 6 m-long bolts can therefore meet the requirements for supporting the EDZ. Thus, the damaged surrounding rock does not entirely lose its load bearing capability. As such, longer bolts (6 m in length) are first used, and then shorter bolts that can penetrate through the relatively thin EDZ are required. If this depth is set to 0.5 m, a

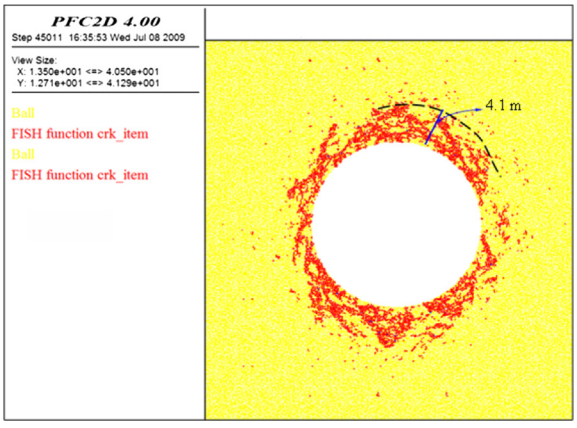

Fig. 15. Simulated damage distribution of surrounding rocks at a depth of 2400 m.

Table 3
PFC analysis results of the depth of fracture-induced damage for marble at different depths.

Depth (m)	EDZ depth (m)
1900	3.1
2000	3.3
2100	3.5
2200	3.7
2300	3.9
2400	4.1
2500	4.2

combination of 4.5 m-long bolts and 6 m-long bolts can meet this requirement.

3.2. Selection of support system

Selecting the appropriate type of support system requires full understanding of its mechanical behaviors. For example, the Swellex bolt is a friction-type bolt that relies on the friction between the surrounding rock and the bolt to provide support. This type of bolt can be quickly installed, which is suitable for rapid support during the excavation of tunnel segments with a high risk of rockburst and large cross-sections. However, such tunnel segments are also highly susceptible to the fracture of the surrounding rocks. Under this condition, if a Swellex bolt is used, the surface support and the anchoring force at the deep water-swelling segment must work together to maintain the stability of the thin layer of fractured rock. This places challenging demands on the strength of the surface support, the bearing plate, and the anchoring force of the Swellex bolt.

3.2.1. Supporting bolts

For the diversion tunnels at the Jinping II hydropower station, the characteristics of different bolts were compared in consideration of various factors, such as the speed and difficulty of installation, and the efficiency of on-site construction. Through testing, the Swellex bolt, the regular mortar bolt, and the expanding-shell prestressed bolt were employed on the construction sites. Through field tests and assessment of the overall effects of the three bolt types, it was determined that (i) the Swellex bolt can be used as the random bolt, and was most suitable for rockburst prevention and control; (ii) the local expanding-shell prestressed bolt was most appropriate for use as permanent support; and (iii) the regular mortar bolt was most appropriate for use as local permanent support at later stages of excavation.

3.2.2. Supporting concrete

Field tests were performed using various new types of concretes. Based on the results of these tests, silica fume and steel fiber concrete were used as the primary types of supporting shotcrete. For general high-geostress tunnel segments, addition of silica fume and steel fiber to the shotcrete allowed the thickness of the primary lining to be reduced. Moreover, the shotcrete hardens rapidly. In this way, the deformation, relaxation, and failure of the surrounding rocks were effectively controlled.

3.2.3. High-pressure and seepage-proof consolidation grouting

In the construction process of the diversion tunnels at Jinping II project, the consolidation grouting for different surrounding rock materials was classified into four types, based on geological conditions and engineering requirements. The first type is a regular consolidation grouting employed for fractured surrounding rocks, in order to improve the mechanical behavior and load bearing capacity of the rock mass, and to increase the impermeability of the surrounding rocks. The second type is the consolidation grouting employed for karst tunnel segments, which is used for prevention to the leakage of internal water from leaking out after completing the backfilling of concrete or mortar in the cavern. The third type is a high-pressure and seepage-proof consolidation grouting. It is the primary method for counteracting the high external water pressure around the tunnel, controlling the stability of the seepage, and reducing the amount of seepage. The fourth type is a shallow consolidation grouting, which is designed specifically for the widespread occurrence of relaxation, fracture, swelling, and failure of the thin damaged layer in brittle marble tunnels under high geostress. The shallow consolidation grouting combined with a secondary lining provides a condition of triaxial pressure for the deep surrounding rocks. This can increase the load bearing capacity of the surrounding rocks, and also improves their anti-seepage-proof performance.

3.2.4. Lining structure

Given that under high geostress, the fracture-induced damage to the surrounding rocks is widespread and suffers continued fracture with elapsed time. In this regard, the long-term stability and safety of anchor-plate retention cannot be guaranteed. Thus, in deep tunnel segments with high geostress, a reinforced concrete lining is employed in combination with shallow consolidation grouting to reinforce the surrounding rocks. This ensures that the load, internal and external water pressures were effectively transferred to the surrounding rocks. Meanwhile, a high confining pressure is applied to the surrounding rocks, preventing the development of internal rock mass relaxation, and improving the peak and residual strengths of the surrounding rocks under the triaxial confining pressure.

3.2.5. External water pressure reduction technology

To ensure the long-term safe operation of deep tunnels, a drainage tunnel is basically constructed between the diversion tunnel and the auxiliary tunnel for discharge of groundwater. Under extreme conditions such as rainstorms, the external water pressure often increases sharply over a short period of time. To address this problem, the consolidation grouting is applied to the diversion tunnel to form an impermeable ring. In addition, the water pressure relief holes are arranged in the lining structure in order to rapidly balance and discharge the external groundwater, so that the external water pressure on the outer margin of the lining is maintained within an allowable range according to the design. This ensures that the lining structure will not collapse due to excessive external water pressure.

4. Comprehensive rockburst prevention and control

The diversion tunnels at the Jinping II hydropower station cut through the Jinping Mountain. The maximum overburden pressure is approximately 69.94 MPa (the maximum depth of 2525 m). In most regions of the construction area, the strength to stress ratio of marble is generally less than 2. The majority of the construction area therefore meets the conditions for the occurrence of rockburst, which is the predominant threat confronted during diversion tunnel construction. An example is presented in Fig. 16.

4.1. Rockburst mechanism and conditions

The rockburst mechanism has become an issue of great concern in rock mechanics, and has been the focus of a considerable number of studies (Kaiser et al., 1996a; Cai et al., 2001b; Feng et al., 2013). However, systematic investigation into the mechanism of rockburst

Fig. 16. An example of strong rockburst in a deep tunnel of the Jinping II project.

in the field is rarely reported. The Canadian Rockburst Research Program (CRRP) has divided rockburst into three types according to their causes, i.e. strain burst, tectonic burst, and pillar burst (Kaiser et al., 1996b; Kaiser and Cai, 2012).

4.1.1. Strain burst

Strain burst can be considered as a severe explosive disaster that occurs when a concentrated stress exceeds the rock strength, and the sudden release of energy in relatively intact brittle surrounding rocks causes rock failure. Strain burst is accompanied by crisp sound, and the possible ejection of rock segments.

In the deep tunnels of the Jinping II project, the initial geostress level of the rock mass generally increases with increasing depth, and thus the risk of strain burst also increases. In Fig. 17a, the tunnel depth is 1300 m, and the maximum depth of rock failure caused by strain burst is 30 cm. In Fig. 17b, the tunnel depth is 1500 m, and the depth of rock failure caused by strain burst is as great as 40 cm. The inset of Fig. 17b illustrates the resulting failure with respect to the tunnel outline.

(a) At a depth of 1300 m.

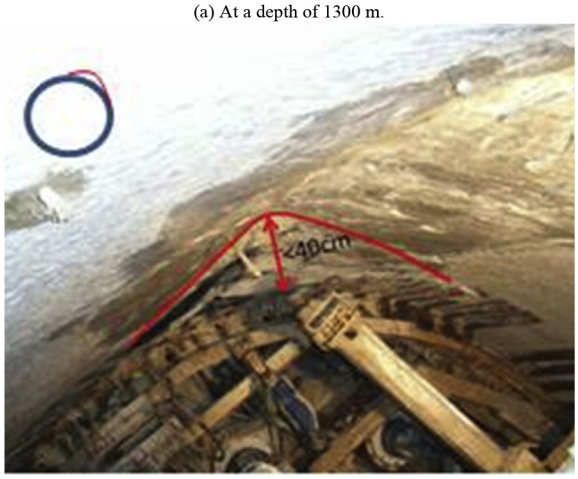

(b) At a depth of 1500 m.

Fig. 17. Spalling events observed at different tunnel depths.

4.1.2. Tectonic burst

Tectonic burst results from structural slippage along a fault, and the sudden release of accumulated high energy leads to local rock mass failure (Zhou et al., 2015). Hence, for the occurrence of tectonic burst, the following two basic conditions must be met:

(1) The distribution of the forces on the geologic structure must be conducive to energy accumulation. At the start of underground excavation, the forces upon the geologic structure tend to be compressive and shear stresses. The maintenance of a sufficient confining pressure meets the requirement of energy accumulation, and the potential shear slip provides the load of the slip failure.
(2) The geologic structure must have the ability to accumulate energy. For a geologic structure filled with weak and soft materials, the energy of compressive and shear stresses upon the geologic structure can be dissipated through compression of the weak filling, and energy does not accumulate. Thus, tectonic burst tends to be generated along the surfaces of hard geologic structures. In particular, in the case of an undulating surface structure or intermittent development, the undulating region of the rock bridge becomes the site of energy accumulation.

The rock mass along the deep tunnels of the Jinping II project exhibits numerous geologic structures in different directions, sizes, and states, as illustrated in Fig. 18. However, not all of these structures can induce tectonic burst, and in fact only two groups of geologic structures are related to tectonic burst. One group is the steep joints with a dip direction toward the northeast, almost perpendicular to the axial direction of the tunnel. The other group is the moderate to low dip angle joints in the northeast direction.

Fig. 18. An example of tectonic burst in a deep tunnel of the Jinping II project.

4.1.3. Pillar burst

To reduce construction time, tunnel excavations often begin from opposite sides and meet in the middle. However, in tunnel segments with high risk of rockburst, as the thickness of the rock pillar between the opposite tunnel faces is reduced, the stress fields in the rock pillar become increasingly superimposed, leading to increasing stored strain energy. When the stored strain energy exceeds a given threshold, pillar burst will occur.

Rock pillars were inevitably formed during construction of the deep tunnels of the Jinping II project, as opposing excavation activities approached one another. As shown in Fig. 19, the auxiliary tunnels A and B cross each other in different parts of the core of Jinping Mountain. When the two opposing tunnel faces were about 50 m apart, severe rockburst was observed during the excavation of the rock pillar.

4.2. Comprehensive rockburst early-warning

Currently, many rockburst early-warning methods have been developed; yet only one single method or indicator was adopted in most engineering projects. Because rockbursts occur randomly and suddenly, it is difficult to predict their occurrence by a single method or indicator. It is also difficult to provide an accurate early-warning system that can indicate the level and location of a rockburst event, which remains an unsolved engineering problem, although a large number of helpful practices and trials have been conducted (Feng et al., 2012; Wu et al., 2015). Due to the complex conditions in the deep tunnels of the Jinping II project, including great depth, high geostress, intensive stress relief, and multiple construction methods, rockburst early-warning is especially complex and difficult.

To solve this problem, a variety of rockburst early-warning methods were used, including geological prediction, microseismic monitoring, geophysical testing, numerical analysis, and empirical evaluation, to acquire information for real-time monitoring and early-warning of rockburst events. Specifically, the following measures were employed for the Jinping II hydropower station:

(1) Prior to tunnel excavation, the risk of rockburst was identified by zones according to the geological conditions.
(2) The risk of rockburst was further evaluated based on observed rock damage and failure, other similar conditions of the tunnel segment, and the influence of adjacent tunnel segments excavated.

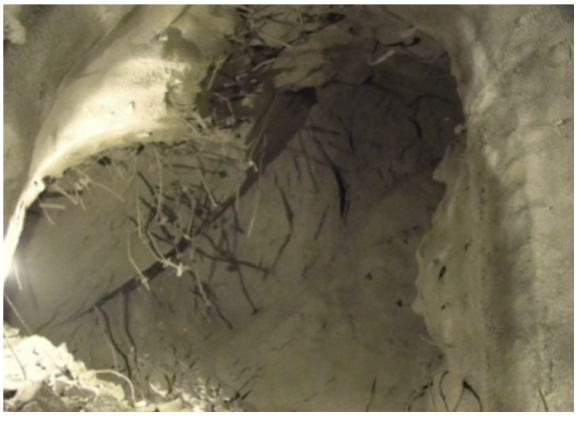

Fig. 19. Failure caused by pillar burst as the opposing excavations of an auxiliary tunnel approach each other.

(3) The risk of rockburst in tunnel segments excavation was also assessed by numerical simulations based on the geological conditions, geostress field distribution, and rock mass behavior. A forecast was then made prior to excavation in combination with the results of Step 2.
(4) The process of rockburst development was monitored and tracked using real-time microseismic monitoring. In this way, precursory seismic events prior to the occurrence of rockburst were acquired, and used in turn for real-time analysis and early-warning. The results were continuously revised to improve the accuracy of the early-warning.

The information acquired from multiple sources was employed according to the above steps to predict the level of rockburst risk, and to establish corresponding countermeasures for avoiding on-site disasters, thereby providing the maximum level of safety for construction personnel.

4.3. Comprehensive method of rockburst prevention and control for DB and TBM excavation

Most moderate to strong rockburst events that occurred during the construction of the diversion tunnels of the Jinping II project were tectonic bursts. Based on the rockburst mechanisms discussed in Section 4.1, we propose the following guideline for comprehensive rockburst prevention and treatment that combines active stress relief with passive control:

(1) The rapid maintenance of the confining pressure on the surrounding rocks in a tunnel to increase their energy storage capacity (Liu et al., 2013a, b).
(2) The causes of energy release, dissipation, and transfer.
(3) Improving the ability of the rock support system to absorb energy and adapt to deformation.

According to the above guideline, the overall principles of support design for the purpose of rockburst prevention and control can be summarized as follows:

(1) The surrounding rocks should always be the main load-bearing structure.
(2) The nano-shotcrete and Swellex bolt support should closely follow the tunnel face to maintain the confining pressure as much as possible. This can limit the extent of fracture propagation in the surrounding rocks, and effectively utilize the ductility of marble.
(3) Take full advantage of the arch effect of the excavated tunnel face, and promptly install expanding-shell prestressed bolt support along the tunnel face to control rock failure induced by high geostress.
(4) Employ the anchor-plate retaining system as subsequent support for comprehensive reinforcement of EDZs.

4.3.1. DB excavation

When tunneling using the DB method, timely active stress relief and effectively passive support control were combined to ensure safety when constructing deep tunnel segments with a high risk of rockburst.

(1) Active stress relief

The artificial intervention of active stress relief is employed to interfere with the stress concentration state inside the rock mass ahead of the tunnel face to ensure the safety of subsequent

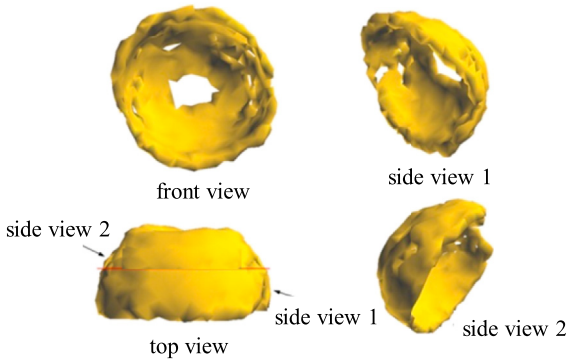

Fig. 20. 3D view of the stress distribution near an excavated rock face.

construction. The active stress relief method employed mainly included modification in the shape of the tunnel face, and stress relief blasting.

Modifying the shape of the tunnel face affects the distribution of high stress zones in the vicinity of the tunnel face, as illustrated in Fig. 20. Adapting the shape of the excavation face to the stress distribution pattern helps to maintain the strength of the surrounding rocks for controlling rockburst by maintaining the level of the confining pressure.

Successful application of stress relief blasting, as illustrated in Fig. 21, can help to dissipate stress concentrations residing ahead of the tunnel face and surrounding the region through which the tunnel will be subsequently extended, thereby reducing the risk of strong rockburst. In addition, stress relief blasting can be implemented in conjunction with conventional blasting to reduce its impact on the construction schedule.

(2) Support control method

According to the mechanical behaviors of deep marble and supporting systems, the support control methodology for rockburst prevention and control can be summarized as follows:

(i) Rockbolts should have good resistance to the impact of rockburst, and provide a strong supporting system. Studies and practical experience have demonstrated that full-length bolt has the optimal technical and economic advantages in view of durability, supporting force, impact resistance, cost, and convenience.
(ii) The support measures must be used to ensure construction safety. Through field practice and exploration, we selected a combination of fast Swellex bolts and mechanical expanding-shell prestressed bolts. These two types of bolts can provide a rapidly installed support to the surrounding rocks.
(iii) The support measures must be systematic and adapt to the characteristics of unloading on the surface of the surrounding rocks under high geostress, and reduce the damage caused by rockburst. All bolts employed in the support system are using steel plates. These plates can be pressed tightly against the steel mesh or the shotcrete layer to increase the supporting effect of the bolts. In this way, the bolts, the steel mesh, and the shotcrete form an integrated structure. An integrated load bearing support system functioning from the inside to the surface of the surrounding rocks is therefore established.
(iv) Nano-materials added to the shotcrete can improve its fast hardening capability, thereby increasing the thickness of each shotcrete layer. Steel fibers or organic imitation steel fibers added to the shotcrete can enhance the capacity of the shotcrete layer to resist the impact of rockburst. These added materials further increase the supporting force on the surface of the surrounding rocks.

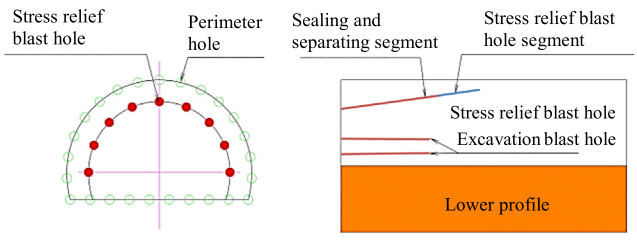

Fig. 21. Stress relief blasting procedure.

Through continuous field tests and various practices, the combined support system is ultimately established as follows. For the prompt covering of the exposed rock surface with shotcrete containing nano-materials, steel fibers, or organic imitation steel fibers, water-swelling random bolts are applied for rapid application of a supporting force. Then, mechanical expanding-shell prestressed bolts are installed near the tunnel face, and serve as a local permanent support. Finally, regular mortar bolts with outer plates and steel mesh, and secondary shotcrete reinforced with nano-materials, steel fibers, or organic imitation steel form a permanent support system that remains some distance behind the tunnel face.

4.3.2. TBM excavation

The general principle of combining active stress relief with support control is also followed for TBM excavation. The initiation of proactive prevention as well as control procedures and measures can avoid strong rockburst during TBM excavation as possible. The catastrophic rockburst-induced surrounding rock collapses that may have severe effects on construction personnel safety and TBM excavation should be eliminated.

(1) Low to moderate risk of rockburst

TBM excavation offers few active measures for rockburst control, and their effects are rather limited. Because the application of stress relief blasting to the tunnel face is impossible with this method, adjustment of the tunneling parameters is the main active measure for rockburst control during TBM excavation. By decreasing the tunneling speed, adjusting the cutter pressure, and using other measures, the disturbance caused by TBM excavation to the surrounding rocks can be reduced, thereby reducing the risk of rockburst.

Targeted support measures are also applied. The prompt application of supporting structures to the surrounding rocks is achieved by using flexible steel mesh, applying nano-organic imitation steel fiber reinforced shotcrete, installing mechanical expanding-shell hollow prestressed or Swellex bolts, and other new materials and technologies.

(2) High risk of strong rockburst

To ensure the safety of equipment and construction personnel when employing TBM excavation for tunnel segments characterized by a high risk of strong to extremely strong rockburst, the rockburst control plan for safe TBM tunneling was implemented as illustrated in Fig. 22. In such tunnel segments, the DB method was first adopted to excavate a pilot tunnel, which was used to release

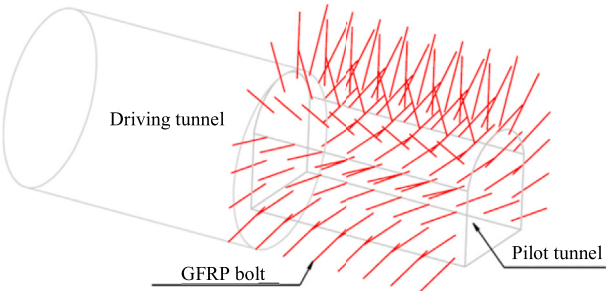

Fig. 22. Excavation of an advanced pilot tunnel in tunnel segments at high risk of strong to extremely strong rockburst.

high geostress in advance. The pilot tunnel also served as an advanced geological exploration tunnel, as well as a working face for advanced preprocessing and microseismic monitoring. The pilot tunnel therefore provided a practical platform for advanced detection, monitoring, analysis, and processing of strong to extremely strong rockbursts prior to TBM excavation. The pilot tunnel scheme can effectively overcome the limits against strong rockburst when using TBM excavation.

5. Identification and treatment for high external water pressure and large-volume groundwater infiltration

As illustrated in Fig. 23, groundwater conditions during the excavation of the diversion tunnels of the Jinping II project were characterized by high pressure, large volume, and variable inflows. For the 5 km-long test tunnel, the maximum external water pressure was 10 MPa. During the construction of the diversion tunnels, 42 exposed groundwater infiltration points having a groundwater inflow greater than 0.05 m^3/s were observed. Among these 42 points, 7 infiltration points had a groundwater inflow greater than 1 m^3/s, and the maximum single-point groundwater inflow was 4.17 m^3/s. In the auxiliary tunnel, the maximum single-point groundwater inflow was 7.3 m^3/s. Water infiltration not only affects the safety and stability of the lining structure of the hydraulic tunnels, which poses a technical challenge for the design of deep tunnel support structures, but also introduces substantial difficulties, which severely delays the progress of construction (Wu et al., 2007).

The following principles should be used during the construction of diversion tunnels to address the issue of groundwater: (i) excavation was performed after hydrogeological exploration; (ii) the blocking of infiltration points was combined with groundwater discharge; (iii) groundwater discharge was then controlled; and (iv) groundwater plugging at a good opportunity. For infiltration points exhibiting high-pressure and large-volume groundwater flow, we should consider whether or not infiltration blocking efforts are able to meet the requirements of the construction project, and whether or not the requirements for the concrete lining can be met to provide adequate conditions for subsequent construction. In addition, the adverse effect of a rising groundwater level on the stability of the surrounding rocks after the blockage of large infiltration points should also be considered.

Fig. 23. An example of high-pressure and large-volume groundwater infiltration during tunnel excavation.

5.1. Techniques for hydrogeological exploration in the alpine-gorge karst region

Carbonate rock formations are widely distributed in the vicinity of the Yalong River bend. Due to the distinctive nature of this area, the degree of karst development is relatively weak, and the typical karst morphology is rarely observed. Through systematic investigation of the site-specific geological conditions, karst development, karst water dynamics, karst water tracing test, and high-pressure and low-temperature corrosion tests on marble, the construction area is divided into various karst hydrogeological units as per the degree of karst development. Examinations of groundwater filling, runoff and discharge in association with 3D seepage flow field analysis of karst development for different karst hydrogeological units were performed. The instantaneous maximum groundwater inflow and stable groundwater inflow in the diversion tunnels were also calculated.

On the basis of the karst hydrogeology, three analytical methods, i.e. hydrogeological analogy method, water balance method, and 3D seepage flow field analysis, were combined to predict the stable groundwater inflow. In the absence of seepage prevention measures, the predicted total steady flow of the two auxiliary tunnels was calculated to be 10–13 m^3/s, and the total steady flow of the seven tunnels of the deep tunnel group was 27.43–29.93 m^3/s. However, in the actual construction, water filling or blocking implemented for some of the infiltration points alters the conditions of the prediction, and hence the prediction results. The external water pressure on the diversion tunnels attained a maximum value of 10 MPa (Ren et al., 2004), which was comparable to the external water pressure on the 5 km-long test tunnel. The maximum single-point groundwater inflow was 5–7 m^3/s.

5.2. Techniques for comprehensive geological forecasting of groundwater

Great attention has been paid to tunnel construction and to determination of the moisture content of the geological body in advance. A number of methods have been developed for detecting karst water and fissure water, including the hydrogeological method, ground penetrating radar (GPR) technology, infrared technology (measuring rock temperature), and the transient electromagnetic method. Among these methods, GPR technology is sensitive to water, which is an effective groundwater search approach. However, the exploration distance from the tunnel surface is relatively short (typically less than 30 m), and data processing and interpretation are difficult. Additionally, GPR is susceptible to interference from metal objects in the tunnel, which can affect the prediction result.

In this case, we established the prediction criteria using various methods, including the formation-relative permittivity assay, the U-shaped test line layout method, the geological structural surface detection method, the GPR first wave phase method, the tunnel

seismic prediction (TSP) method, and the method for assessing the presence of groundwater infiltration using GPR technology. To further explore the spatial range of water-bearing structures on a fine scale, we employed a method for predicting the existence of water-bearing structures using borehole radar, which is illustrated in Fig. 24. With this method, a spatial range of 30 m in diameter ahead of the tunnel face can be evaluated, and the precision and resolution are far greater than those of standard geophysical methods. As a result, blind spots that cannot be accurately evaluated with regular geophysical methods can also be identified. The advanced, accurate forecasting of groundwater was achieved with a accuracy of 95%.

We also established a comprehensive multi-step forecasting and early-warning system for karst tunnels based on the testing results obtained from macro-geological forecasting (engineering geology methods), long-term geological prediction distances of 50–200 m (engineering geology methods and TSP), and short-term geological prediction distances of 0–50 m (GPR and transient electromagnetic method) (Li et al., 2007). During the construction period, the accuracy of the interpretation was improved by combining on-site feedback obtained for each forecasting step, and a corresponding advanced geological forecasting report was submitted. Appropriate early-warning plans and countermeasures were established accordingly to ensure the safety of tunnel construction.

5.3. Technologies for comprehensive groundwater treatment

The types of groundwater encountered during diversion tunnel construction primarily include seepage drip from fractured rock masses, linear flow, and concentrated infiltration. The treatment for seepage drip and linear flow groundwater is relatively fast and easy due to their low flow rate and pressure. As such, these two types of groundwater have a minor effect on the construction process. In the present project, water plugging was the primary treatment method employed for inhibiting seepage drip and linear flow groundwater, facilitating the construction of the concrete lining. However, much time and effort are required for treating high-pressure concentrated groundwater infiltration points owing to the absence of mature treatment methods, which represents a constraint on safe deep-tunnel construction. To solve this issue, a design of dynamically coordinated exploration, blocking, and discharge was employed based upon a well-established treatment guideline.

For the technical difficulty of treating exposed high-pressure concentrated groundwater infiltration with an inflow less than 1 m^3/s, we employed the diversion decompression technique illustrated in Fig. 25 to reduce the pressure and inflow rate of groundwater at the infiltration points, and to control the water pressure near the infiltration points. This can gradually block the infiltration points, and finally grouting can be used to fully block the strong concentrated groundwater infiltration. A groundwater infiltration point before and after blockage is illustrated in Fig. 26a and b, respectively. With this blocking technique, the construction process is speeded up and the risk of water inrush is reduced. Application of this method has shown that the treatment time was generally reduced by 1–2 months.

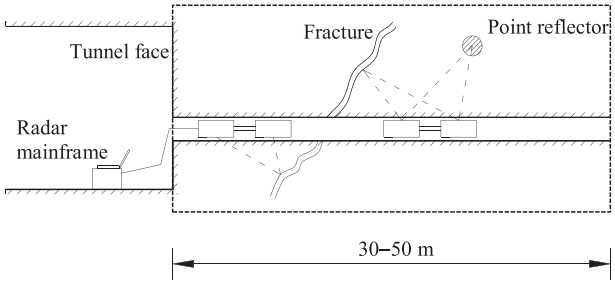

Fig. 24. Prediction of water-bearing structures using borehole radar.

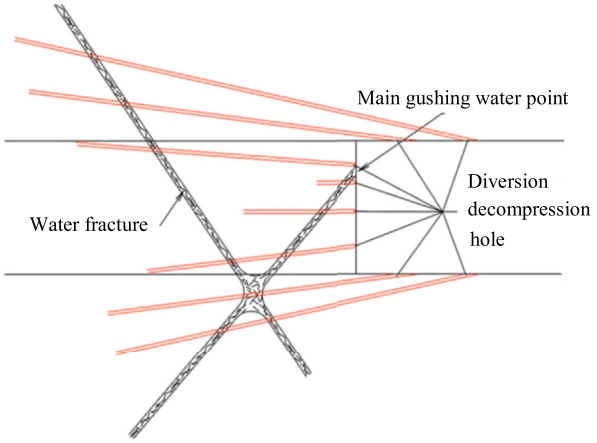

Fig. 25. Diversion decompression grouting for groundwater infiltration blocking.

For the technical difficulty of treating exposed high-pressure groundwater infiltration with an inflow greater than 1 m^3/s, a blocking technique was employed, as illustrated in Fig. 27. This technique allowed the successful blockage of high-pressure groundwater with inflow value of 7.3 m^3/s. The application of this technique also involved the independent development of a grouting technique of mixing cement slurry and water glass outside the hole. Several practical and effective high-pressure grouting devices

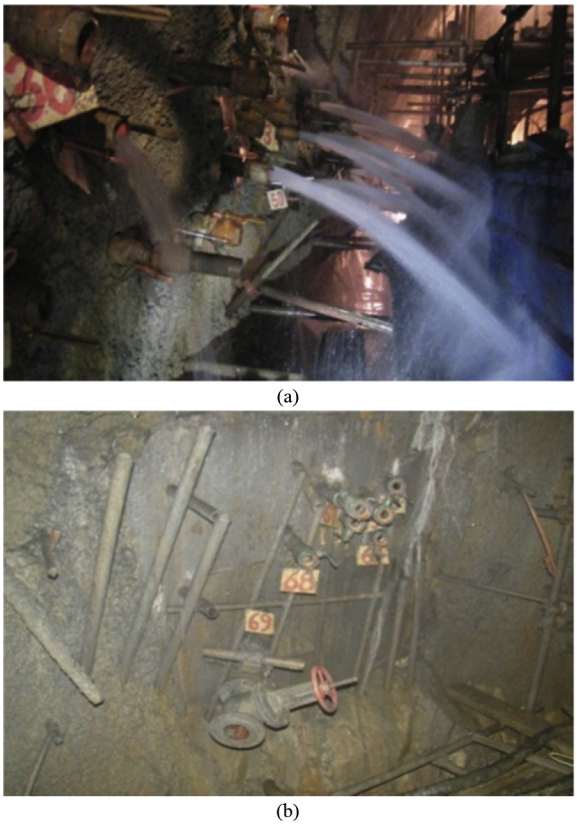

Fig. 26. An example of a concentrated groundwater infiltration point (a) before and (b) after treatment.

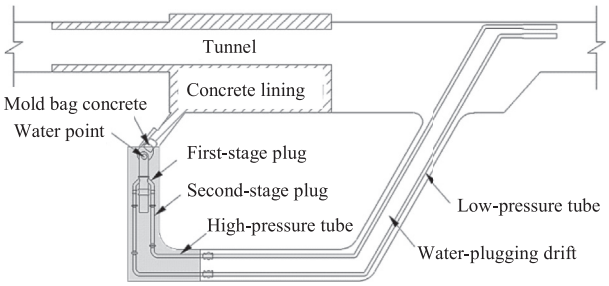

Fig. 27. Blocking of a high-pressure and large-volume groundwater infiltration point.

were developed, including a grout mixing device, a high-pressure grouting plug, and a sealing device. With this set of treatment technologies, we were able to control the grouting solidification time, which greatly improved the anti-dispersion capability of the slurry, and addressed the challenging issue imposed by high-pressure and large-volume groundwater infiltration in the Jinping II project.

6. Conclusions

The Jinping II hydropower station has been operating in good condition since it was completed in 2014. According to the inspection results obtained during diversion tunnel construction, as well as the monitoring data obtained during operation, the stress and deformation of the bolts, the stress of the reinforcement in the concrete lining, and the concrete lining strain are all stable. The maximum external water pressure obtained from osmometer measurements meets the requirements of structural safety. No failure has been observed along the diversion tunnels during operation. This suggests that the measures used to treat various major risks encountered during project construction have ensured the stability and structural safety of the surrounding rocks. The achievements can be summarized as follows:

(1) Nondestructive sampling technology has been developed to investigate the characteristics of cracking and initial damage to rock cores caused by unloading under high geostress. Techniques for in-situ testing of deep rocks, which are primarily based on AE monitoring, stress monitoring, optical fiber Bragg grating monitoring, and acoustic wave velocity testing, have been developed and employed. The developed nondestructive sampling and in-situ measurements were employed to fully characterize the formation and development of EDZs, and to evaluate the mechanical behaviors of deep rock masses at multi-scale with high-precision.

(2) The time effect of marble fracture propagation, the brittle–ductile–plastic transition of marble, and the temporal development of rock mass fracture and damage induced by high geostress have been characterized. A brittle–ductile–plastic transition constitutive model based on the Hoek–Brown failure criterion was established for accurate simulation of the complex mechanical behaviors of deep rocks.

(3) On the basis of understanding of the interaction between the support and the surrounding rocks under high geostress conditions, appropriate types of support systems were selected, and a combined load bearing system was designed.

(4) The mechanism of rockburst, e.g. strain burst, tectonic burst, and pillar burst has been identified, and a rockburst risk early-warning system that integrates geological forecasting, microscopic interpretation, microseismic monitoring, and empirical assessment was developed. The safe construction of deep tunnels was achieved under a high risk of strong rockburst using active measures, such as stress relief blasting, tunnel face modification, and the use of pilot tunnels, to dissipate and transfer the energy accumulated in the surrounding rocks.

(5) Techniques for the survey of karst hydrogeological conditions in the alpine-gorge region were combined with methods for the fine exploration of water-bearing structures to establish an integrated forecasting and early-warning system for evaluating the risk of catastrophic groundwater infiltration events during the process of deep tunnel construction. A complete set of technologies for treatment of high-pressure and high-volume groundwater infiltration has been developed.

Conflict of interest

The authors wish to confirm that there are no known conflicts of interest associated with this publication, and there has been no significant financial support for this work that could have influenced its outcome.

Acknowledgments

The financial support provided by the HydroChina Scientific Research Project (GW-KJ-2013-11) is gratefully acknowledged.

References

Cai M, Kaiser PK, Martin CD. Quantification of rock mass damage in underground excavations from microseismic event monitoring. International Journal of Rock Mechanics and Mining Sciences 2001a;38(7):1135–45.

Cai MF, Wang JA, Wang SH. Analysis of energy distribution and prediction of rockburst during deep mining excavation in Linglong gold mine. Chinese Journal of Rock Mechanics and Engineering 2001b;20(1):38–42 (in Chinese).

Chen BR, Feng XT, Xiao YX, et al. Acoustic emission test on damage evolution of surrounding rock in deep-buried tunnel during TBM excavation. Chinese Journal of Rock Mechanics and Engineering 2010;29(8):1562–9 (in Chinese).

Chu WJ, Zhang CS, Chen PZ, et al. In-situ test on diversion tunnel at Jinping II hydropower station. II – analysis of results. Chinese Journal of Rock Mechanics and Engineering 2014;33(8):1702–10 (in Chinese).

Fairhurst C. Nuclear waste disposal and rock mechanics: contributions of the underground research laboratory (URL), Pinawa, Manitoba, Canada. International Journal of Rock Mechanics and Mining Sciences 2004;41(8):1221–7.

Feng XT, Chen BR, Zhang CQ, Li SJ, Wu SY. Mechanism, warning and dynamic control of rockburst development process. Beijing, China: Science Press; 2013 (in Chinese).

Feng XT, Zhang CQ, Chen BR, et al. Dynamical control of rockburst evolution process. Chinese Journal of Rock Mechanics and Engineering 2012;31(10):1983–97 (in Chinese).

Kaiser PK, Cai M. Design of rock support system under rockburst condition. International Journal of Rock Mechanics and Mining Sciences 2012;4(3):215–27.

Kaiser PK, McCreath DR, Tannant DD. Canadian rockburst support handbook: Volume 2: Rockburst support. In: Canadian Rockburst Research Program 1990–1995. Sudbury, Ontario, Canada: Canadian Mining Industry Research Organization (CAMIRO); 1996b.

Kaiser PK, Tannant DD, McCreath DR. Drift support in burst-prone ground. CIM Bulletin 1996a;89(998):131–8.

Li SC, Li SC, Zhang QS, et al. Forecast of karst-fractured groundwater and defective geological conditions. Chinese Journal of Rock Mechanics and Engineering 2007;26(2):217–25 (in Chinese).

Liu N, Zhang CS, Chu WJ, Wu XM, Zhang CQ. Influence of mechanical characteristics of deep-buried marble on rockburst occurrence conditions. Rock and Soil Mechanics 2013a;34(9):2638–42 (in Chinese).

Liu N, Zhang CS, Chu WJ, Wu XM. Microscopic characteristics analysis of brittle failure of deep buried marble. Chinese Journal of Rock Mechanics and Engineering 2012a;9(Suppl. 2):3557–65 (in Chinese).

Liu N, Zhang CS, Chu WJ. Detection and analysis of excavation damage zone of deep tunnel. Rock and Soil Mechanics 2011a;32(Suppl. 2):526–31 (in Chinese).

Liu N, Zhang CS, Chu WJ. Experimental research on time-dependent behavior of crack propagation in Jinping deep marble. Rock and Soil Mechanics 2012b;33(8):2437–43 (in Chinese).

Liu N, Zhang CS, Chu WJ. Simulating time-dependent failure of deep marble with particle flow code. Chinese Journal of Rock Mechanics and Engineering 2011b;30(10):1989–96 (in Chinese).

Liu N, Zhang CS, Wu XM, Chu WJ. Time-dependent failure of deep-buried marble in Jinping II hydropower station. Advances in Science and Technology of Water Resources 2013b;33(2):63–7 (in Chinese).
Malmgren L, Saiang D, Toyra J, Bodare A. The excavation disturbed zone (EDZ) at Kiirunavaara mine, Sweden by seismic measurements. Journal of Applied Geophysics 2007;61(1):1–15.
Martino JB, Chandler NA. Excavation-induced damage studies at the underground research laboratory. International Journal of Rock Mechanics and Mining Sciences 2004;41(8):1413–26.
Potyondy DO, Cundall PA. A bonded-particle model for rock. International Journal of Rock Mechanics and Mining Sciences and Geomechanics Abstracts 2004;41(8):1329–64.
Potyondy DO. Simulating stress corrosion with a bonded-particle model for rock. International Journal of Rock Mechanics and Mining Sciences 2007;44(5):677–91.
Read RS. 20 years of excavation response studies at AECL's underground research laboratory. International Journal of Rock Mechanics and Mining Sciences 2004;41(8):1251–75.
Ren XH, Wang MQ, Wang SH, Liu L. Study on the external water pressure of deep lying tunnel in Jinping Hydropower Station. Hydrogeology and Engineering Geology 2004;31(3):85–8 (in Chinese).
Wu SY, Wang J, Wang G. Underground water and its treatment strategy in auxiliary tunnels of Jinping hydropower project. Chinese Journal of Rock Mechanics and Engineering 2007;26(10):1959–67 (in Chinese).
Wu SY, Zhou JF, Chen BR, Huang MB. Research on effects of excavation schemes of TBM on risk of rockburst of long power tunnels of Jinping II hydropower station. Chinese Journal of Rock Mechanics and Engineering 2015;34(4):728–34 (in Chinese).
Zhang CS, Chen XR, Chu WJ, Zhu YS, Zhu HC. Behavior of marble at Jinping II project – Part 2: rock mass. In: Proceedings of the 44th US Rock Mechanics Symposium and 5th US-Canada Rock Mechanics Symposium. Alexandria, Virginia, USA: American Rock Mechanics Association; 2010. p. 2014–20.
Zhang CS, Chen XR, Hou J, Chu WJ. Study of mechanical behavior of deep-buried marble at Jinping II hydropower station. Chinese Journal of Rock Mechanics and Engineering 2010b;29(10):1999–2009 (in Chinese).
Zhang CS, Chu WJ, Hou J, Chen XR, Wu XM, Liu N. In-situ test on diversion tunnel at Jinping II hydropower station. I – test design. Chinese Journal of Rock Mechanics and Engineering 2014;33(8):1691–701 (in Chinese).
Zhang CS, Chu WJ, Liu N, Zhu YS, Hong J. Laboratory tests and numerical simulations of brittle marble and squeezing schist at Jinping II hydropower station, China. Journal of Rock Mechanics and Geotechnical Engineering 2011;3(1):30–8.
Zhang CS, Liu N, Zhu HC, Chu WJ, Wu JY. Time-dependent behavior of crack propagation and evaluation of control effect of Jinping deep marble. Chinese Journal of Rock Mechanics and Engineering 2013;32(10):1964–72 (in Chinese).
Zhang CS. Study on technical cruxes of diversion tunnels of Jinping II hydropower project on Yalong River. China Investigation and Design 2007;8:41–4 (in Chinese).
Zhou H, Meng MZ, Zhang CQ, Lu JJ, Xu RC. Analysis of the structural plane controlling mechanism on rockburst in deep hard rock tunnels. Chinese Journal of Rock Mechanics and Engineering 2015;34(4):720–7 (in Chinese).

Chunsheng Zhang graduated from Zhejiang University in 1985, and obtained his master's degree from Southwest Jiaotong University in 1993. He is now the Dean of HydroChina Huadong Engineering Corporation, Member of Chinese Society for Rock Mechanics and Engineering, Vice President of Zhejiang Province Society of Hydroelectric Engineering, Member of Chinese Hydraulic Engineering Society. His research interests cover water resources and hydropower engineering. Prof. Zhang participated in more than 20 large and medium hydropower stations' design and technical work, such as Jinping II, Baihetan, Tongbai, Taian, Yixing projects in China. He was the recipient of the Chinese Good Design Gold Award in 2004, and won the Second Class Prize of National Scientific and Technological Progress in 2013 and 2014, respectively.